GEANT4 Simulation of the Jlab MeV Mott Polarimeter

Martin McHugh
The George Washington University
mjmchugh@jlab.org

2016-02-26

Abstract

The simulation of the JLab Mott Polarimeter, constructed using GEANT4, represents the physical geometry of the polarimeter, and is capable of reproducing results seen in the physical apparatus. As such, it is a powerful tool with which to describe the polarimeter. In particular we use the simulation to determine the effect of single Mott scattering and double Mott scattering as a function of target thickness. These results provide a model driven fit of the effective Sherman function.

1 JLab Polarimeter and Mott Scattering

The MeV Mott Polarimeter is located in the Continuous Electron Beam Accelerator Facility (CEBAF) injector at Jefferson Lab (JLab). It is used to measure the transverse polarization of the electron beam in the 2 - 10 MeV energy range. The polarimeter measures the elastic scattering asymmetry of electrons incident on the nuclei of a thin target foil. The foils used include gold, silver, and copper and range in thickness from 100-10,000 Å. The elastically scattered electrons pass through aperatures of an aluminum collimator that defines the scattering angle of $172.6^\circ \pm 0.1^\circ$ with a per quadrant solid angle of 0.18 msr. The scattered electrons pass then pass through the 0.2032 mm (8 mil) thick aluminum window and into the detector packages. Each detector package contains two plastic scintillators connected to PMTs for readout: a 1 mm $\times$ 25.4 mm $\times$ 25.4 mm wafer scintillator, the Δ E detector, and a cylindrical 76.2 mm diameter, 63.5 mm long scintillator, the E detector, which functions as a stop detector and calorimeter with a 3% energy resolution.

1.1 Mott Scattering

The polarimeter functions by measuring the Mott scattering asymmetry. Mott scattering describes elastic electron-nuclear scattering. The differential cross-section can be written as

$$\frac{d\sigma}{d\Omega}(\theta) = I(\theta)\left(1 + S(\theta)\vec{P}\cdot\hat{n}\right) \tag{1}$$

where $I(\theta)$ is the spin independent form of the Mott cross section, $\vec{P}$ is the incoming beam's polarization, $S(\theta)$ is known as the Sherman function and

$$\vec{n} = \frac{\vec{p}\times\vec{p}\,'}{|\vec{p}\times\vec{p}\,'|} \tag{2}$$

where $\vec{p}$ ($\vec{p}'$) is the incoming (outgoing) momentum of the electron. In the case of ideal single scattering we expect to measure an asymmetry,

$$A = \frac{N_L - N_R}{N_L + N_R} = P_y S(\theta_{sc}) \tag{3}$$

where $N_{L(R)}$ is the number of hits in the left(right) detector placed at a scattering angle, θ_{sc}. However, the asymmetry we actually observe depends on target thickness and is averaged over the acceptance of our detectors. This produces an "effective" Sherman function, $S_{eff}(\theta, d\Omega, d)$, where $d\Omega$ is the detector acceptance and d is the target thickness. The solid angle is fixed for the polarimeter and can be dealt with by averaging the Sherman function over the acceptance. The target thickness dependence is clearly shown in Fig. 1. This target thickness dependence is suspected to be due to electrons that undergo multiple Mott scatterings within our target. The goal of the `GEANT4` simulation is to see if we can reproduce the effective Sherman function in order to verify our polarimeter's accuracy.

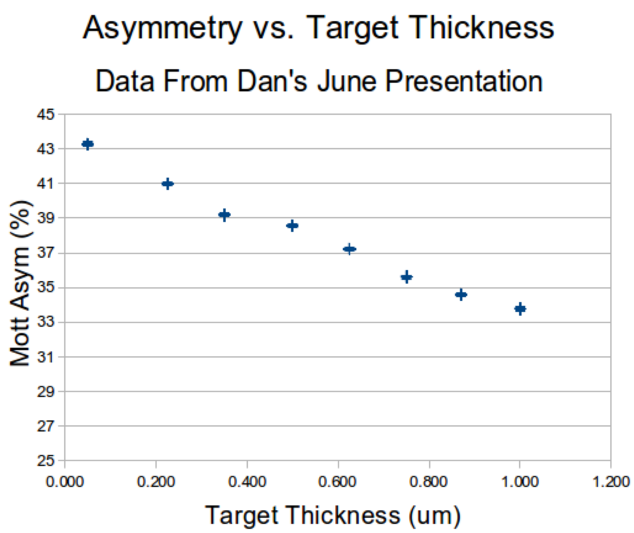

Figure 1: Data from the target foils indicating the change of the asymmetry with target thickness.

1.2 Double Mott Scattering

It is our assumption that the target thickness dependence of the Mott scattering asymmetry is the result of multiply scattered electrons within the target foil. Simulation of this effect requires us to track the polarization over multiple steps. A Mott scattered electron beam carries a new polarization.

$$\vec{P}^{\dagger} = \frac{\left(\vec{P} \cdot \vec{n} + S(\theta)\right) \vec{e}_1 + U(\theta)\vec{e}_2 + T(\theta)\vec{e}_3}{1 + \vec{P} \cdot \vec{n}\, S(\theta)} \tag{4}$$

where

$$\vec{e}_1 = \vec{n} \tag{5}$$
$$\vec{e}_2 = \vec{n} \times \vec{P} \tag{6}$$
$$\vec{e}_3 = \vec{n} \times \left(\vec{P} \times \vec{n} \right) \tag{7}$$

and $U(\theta)$ and $T(\theta)$ are functions which measure the spin transfer probability of the scattering. Plots of the relevant scattering functions for a selection of typical energies can be seen in Fig. 2. Those plots are generated using the scattering calculations performed by Xavier Roca-Maza, detailed in [3]. These calculations form the basis of Mott scattering physics in our simulation. One can observe that the JLab Mott Polarimeter was built at the point where the asymmetry is largest rather than at the point where the figure of merit (shown in Fig. **??**) is maximized.

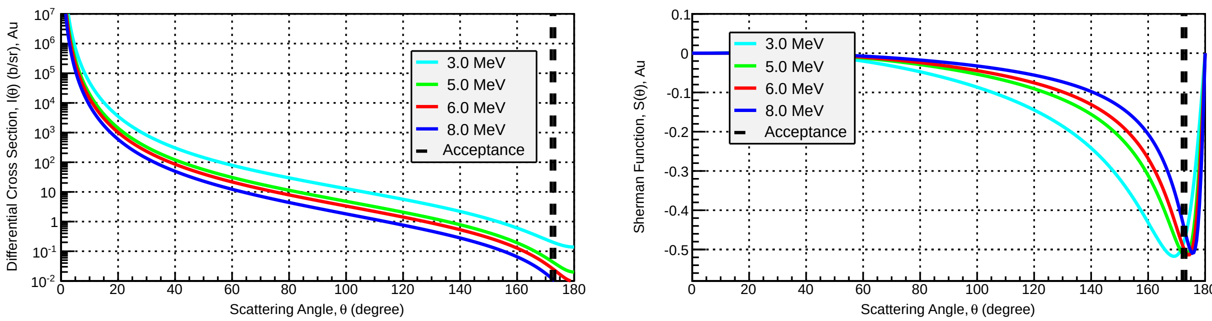

Figure 2: Mott cross section, $\frac{d\sigma}{d\Omega}$, and analyzing power, $S(\theta)$, as a function of scattering angle.

2 Simulating Mott Scattering

To begin our simulation, we must generate electrons in our apparatus to represent certain physical cases. Before we discuss the particular cases the simulation can model in the following sections, we look at the properties of our "incident beam" of electrons on the target.

In all of the following cases, the electron beam is assumed to have an initial polarization. While the user may modify this, the standard assumption made is that the beam is 100% polarized in the positive y direction; $\vec{P}_1 = \hat{\jmath}$. The incident electrons are assumed to have momentum entirely in the z direction; $\vec{p}_1 = p\hat{k}$. The beam is assumed to have a circular, Gaussian profile on the target with a FWHM of 1 mm. All simulations were run with a beam energy of 5.0 MeV and a Gaussian energy spread of 150 keV.

2.1 Single Scattering: Rejection Method

To look at the detector response to electrons that undergo exactly one Mott scattering process in the target, we use the following algorithm:

1. Pick a scattering position, $\vec{x}_1$, within the intersection of the beam and our target.

2. Pick a point, $\vec{x}_2$, in the acceptance the primary collimator.
3. Calculate $\frac{d\sigma}{d\Omega}(\vec{x}_1, \vec{x}_2)$.
4. Rejection sample against this cross-section. If accepted, proceed to generate the event. If rejected repeat steps 1-3.

In order to measure the Mott asymmetry from single scattering simulations generated in this manner, we simply use Eq. (3):

$$\varepsilon_1^{rej.} = \frac{N_{L_1}^{rej.} - N_{R_1}^{rej.}}{N_{L_1}^{rej.} + N_{R_1}^{rej.}} = -0.513 \pm 0.0005 \tag{8}$$

It should be noted that the theoretical single scattering asymmetry is:

$$\varepsilon_1^{th.} = -0.514 \pm 0.003 \tag{9}$$

so we have effectively simulated single Mott scattering. Unfortunately, the results do not change with target thickness confirming that single scattering is not adequate to explain the measurements conducted using thick target foils.

2.2 Double Scattering: Rejection Method

Double scattering refers to Mott scattering from exactly two distinct nuclei within the target foil. The assumption is that this process becomes a more important contribution to the detector signal as target thickness increases. The first method I've used to calculate the effect of double scattering is a rejection method. The algorithm is:

1. Pick a scattering position, $\vec{x}_1$, within the intersection of the beam and our target.
2. Pick a point, $\vec{x}_2$, within the target, such that $|\vec{x}_2 - \vec{x}_1| < 0.16$ mm. Beyond this distance in Gold a 5 MeV electron will lose over 500 keV and no longer be of interest to us.
3. Calculate $\frac{d\sigma_1}{d\Omega_1}(\vec{x}_1, \vec{x}_2)$.
4. Pick a point, $\vec{x}_3$, in the acceptance the primary collimator.
5. Calculate $\frac{d\sigma_2}{d\Omega_2}(\vec{x}_2, \vec{x}_3)$.
6. Rejection sample against this $\frac{d\sigma_1}{d\Omega_1}\frac{d\sigma_2}{d\Omega_2}$. If accepted, generate electron at $\vec{x}_2$ towards $\vec{x}_3$ If rejected repeat steps 1-5.

Simulating 10 million events at each target foil thickness, this method produces an asymmetry of

$$\varepsilon_2^{rej.} = \frac{N_{L_2}^{rej.} - N_{R_2}^{rej.}}{N_{L_2}^{rej.} + N_{R_2}^{rej.}} = -0.011 \pm 0.003 \tag{10}$$

Unfortunately this asymmetry also does not scale with target thickness. The path we will follow from this point on is to see what the relative fraction of the detector signal are come from both single and double scattering.

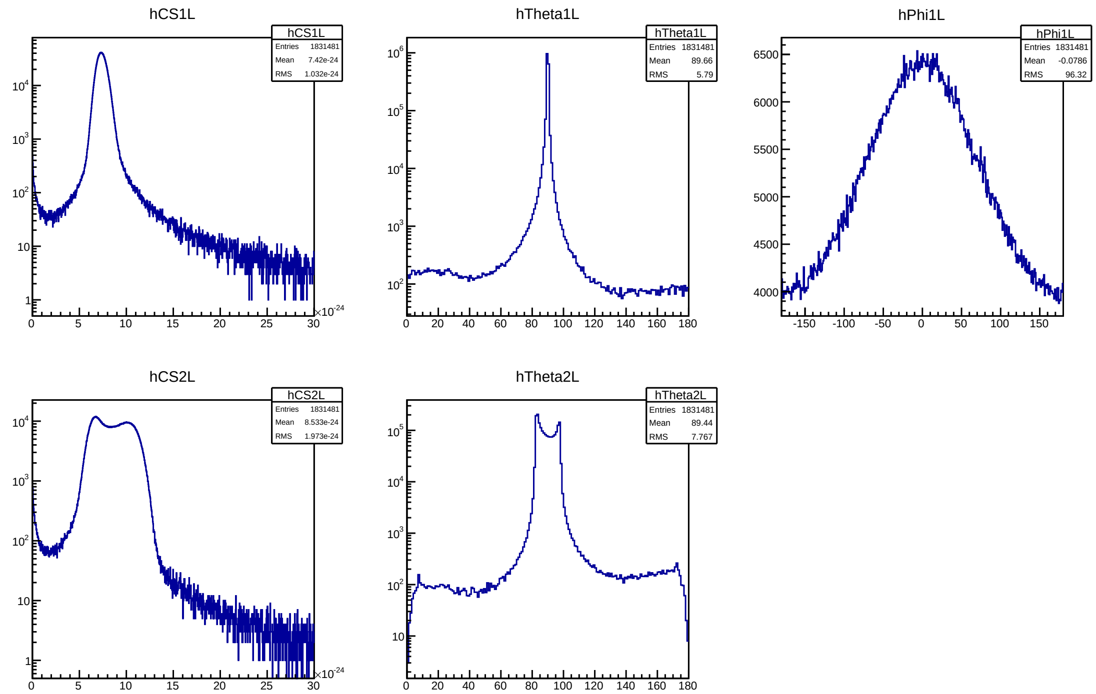

Figure 3: Double scattering information for hits in the left detector. From left to right in the top row, the initial cross-section, scattering angle, and azimuthal angle. The bottom row contains the same information for the second scattering.

2.3 Calculating Rates

In order to proceed, we use the simulation results to calculate predicted rates in each detector for the two processes of intrest. The rate is the simplest quantity with which to compare simulations to data. The rate calculated from a given simulation is a prediction of the number of events that will hit our detector per unit current per unit time, using the assumptions in our simulation. All rates quoted in this note will have units of Hz/μA.

Firstly we will discuss the general method of rate calculation and show how this leads to a form of the effective Sherman function. The differential rate in our detector from one point in phase space, $\vec{v}$, is:

$$d\mathcal{R}(\vec{v}) = \mathcal{L}(\vec{v})\sigma(\vec{v})\epsilon(\vec{v})dv, \tag{11}$$

where $\mathcal{L}(\vec{v})$ is the luminosity, $\sigma(\vec{v})$ is the cross-section of the physics of interest and $\epsilon(\vec{v})$ is the acceptance function of our detectors (essentially the chance that an event near $\vec{v}$ will be detcted). The total rate our detector sees from one processes is simply the integral of Eq. (11):

$$\mathcal{R} = \int_V d\mathcal{R}(\vec{v}). \tag{12}$$

While $\mathcal{L}(\vec{v})$ and $\sigma(\vec{v})$ are often known quantities, $\epsilon(\vec{v})$ is a value obtained solely by simulation.

The numerical solutions of Eq. (12) proposed in the following sections require us to use a generator that does not weight by cross section as the rejection method in sections 2.1 and 2.2. For this purpose a generator was made for each type of event which follows the relevant algorithm but simply omits the final rejection sampling.

2.4 Data Rates

In order to compare our results to data, we first must have a good understanding of that data. This section exists to describe the method for determining scattering rates in our detector. Since the Mott polarimeter's beam flips polarization direction at a rate of 30 Hz, each detector sees a combination of each spin state. Additionally, there are known detector efficiency differences between the four detectors. In order to compare to simulation, data were analyzed so that an average was constructed from all four detectors looking at events which had a coincidence between the E and $DeltaE$ detector, and a timing cut to ensure that the electrons were from the target. The results were fit with a parabola in order to determine linear and quadratic coefficients. The resulting fit $R^{data}(d) = a_1^{data} d + a_2^{data} d^2$ has coefficients,

$$a_1^{data} = 0.19 \pm 0.01 \text{ Hz}/(\mu\text{A nm}), \tag{13}$$

$$a_2^{data} = 70 \pm 17 \ \mu\text{Hz}/(\mu\text{A nm}^2). \tag{14}$$

The data from which these were drawn is shown in Table 1.

d (nm)	$\mathcal{R}^{\text{data}}$	$\mathcal{R}_1^{\text{fit}}$	$\mathcal{R}_2^{\text{fit}}$
52	9.9±0.1	9.8±0.5	0.19±0.05
215	46.5±0.5	40.3±2.1	3.2±0.8
389	82.6±1.0	73.0±3.7	10.5±2.6
487	97.7±1.0	91.3±4.6	16.5±4.1
561	128.7±1.3	105.2±5.3	21.9±5.4
775	178.3±1.9	145.3±7.4	41.7±10.3
837	209.3±2.2	157.0±8.0	48.7±12.1
944	246.0±2.5	177.0±9.0	61.9±15.3

Table 1: From left to right, the data, linear fit, and quadratic fit portions. Data and fit taken from: `https://wiki.jlab.org/ciswiki/images/e/ef/Rates.pdf`. All rates are given in units of Hz/μA.

2.5 Single Scattering Rate: Reimann Integration

For a single scattering event, our phase space vector becomes $\vec{v} = (x, y, z, E, \chi, \psi)$ and the volume element is $dv = dxdydzdEd\chi d\psi$. The total rate in a detector is then:

$$\mathcal{R} = \int_V \mathcal{L}(\vec{v})\sigma(\vec{v})\epsilon(\vec{v}) \sin\chi dv. \tag{15}$$

The integrals over x, y are trivial. Additionally, the dependence of $\sigma(\vec{v})$ upon z and E are small enough to ignore in our case. Figure 4 shows plots of the acceptance function,$\epsilon(\vec{v})$, with respect to the different variables of single scattering. As is demonstrated in the figure, the acceptance function's behavior is well characterized solely by it's dependence upon scattering angle, χ and azimuthal angle ψ. Thus:

$$\epsilon(\vec{v}) = \epsilon(\chi, \psi). \tag{16}$$

Using these simplifications we obtain a rate :

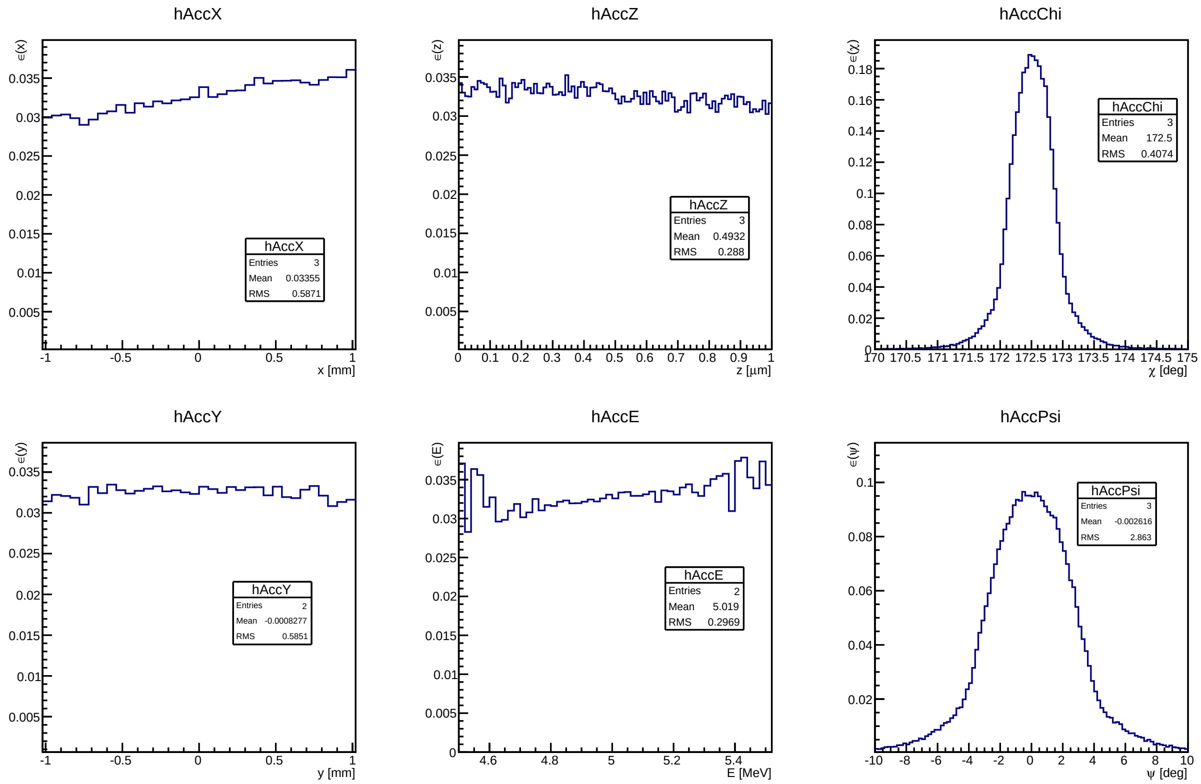

Figure 4: Simulated Acceptance Functions for each of the six degrees of freedom in single scattering. Results are from the Left detector for 10 million events thrown. Only $\epsilon(\chi)$ and $\epsilon(\psi)$ show large dependence.

$$\mathcal{R} = \frac{N_A \rho}{A} N_B d \int_{\psi_{min}}^{\psi_{max}} \int_{\chi_{min}}^{\chi_{max}} \sigma(\chi, \psi) \epsilon(\chi, \psi) \sin \chi d\chi d\psi, \tag{17}$$

Where N_A is Avogadro's number, ρ is the density of the target foil, A is the atomic weight of the foil material, N_B is the number of electrons per second in 1 μA, and d is the target thickness. In order to numerically solve Eq. (17) we perform a Reimann sum. We divide the 2D integral into $N_\chi \times N_\psi$ bins in χ and ψ of size $\Delta\chi\Delta\psi$. In our case we used 350 bins in each variable. Then Eq. (17) can be estimated using

$$\mathcal{R} \approx \frac{N_A \rho}{A} N_B d \sum_{i=1}^{N_\chi} \sum_{j=1}^{N_\psi} \sigma_{ij} \epsilon_{ij} \sin \chi_i \Delta\chi \Delta\psi, \tag{18}$$

Where σ_{ij} is the average cross-section for all events thrown in the ij'th bin and ϵ_{ij} is the acceptance function for the bin. The uncertainty, $\delta\mathcal{R}$, from this method is given by

$$\delta\mathcal{R}^2 = \left(\frac{N_A \rho}{A} N_B d \Delta\chi \Delta\psi \right)^2 \sum_{i=1}^{N_\chi} \sum_{j=1}^{N_\psi} \left(\epsilon_{ij}^2 \delta\sigma_{ij}^2 + \sigma_{ij}^2 \delta\epsilon_{ij}^2 \right) \sin^2 \chi_i. \tag{19}$$

Figure 5 shows the binned cross-section and acceptance function for a run. Using this method gives us the results shown in Table 2. These results allow us to make independent predictions of both the linear coefficient of the rate

$$a_1^{sim.} = \left\langle \mathcal{R}_1^{sim.}/d \right\rangle = 0.198 \pm 0.001 \text{ Hz}/(\mu\text{A nm}), \tag{20}$$

where averaging is carried over all eighteen simulated thicknesses. The asymmetry of single scattering is calculated from rates as follows:

$$\varepsilon_1^{rate} = \left\langle \frac{\mathcal{R}_{L_1} - \mathcal{R}_{R_1}}{\mathcal{R}_{L_1} + \mathcal{R}_{R_1}} \right\rangle = -0.513 \pm 0.006. \tag{21}$$

With a similar averaging procedure. These results are in good agreement with data and theory, respectively.

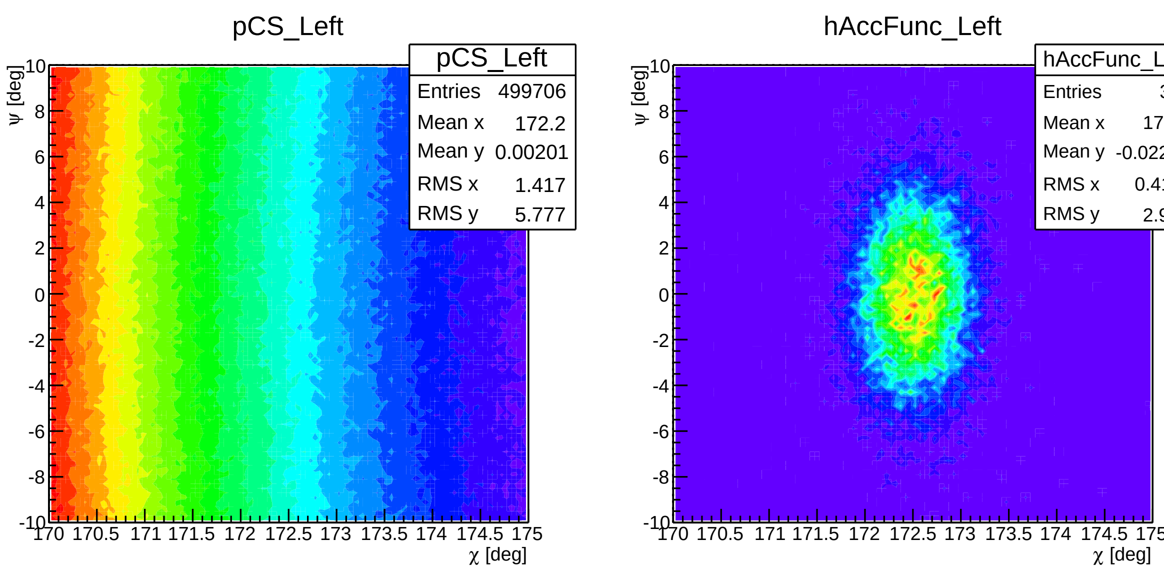

Figure 5: On the left: Simulated average cross-section as a function of scattering angle, χ, and azimuthal angle, ψ, for the left detector. On the right: Simulated acceptance function, $\epsilon(\chi, \psi)$. Results from a simulation of one million events and a 52 nm gold foil.

2.6 Double Scattering Rates

In the case of double scattering, we can't use the Riemann sum method because the phase space is significantly more complicated and the summation needs to be carried out over more dimensions. We turn instead to the idea of Monte Carlo integration using the outputs of the GEANT4 simulation. This method has the advantage of being tractable however, it converges slowly so we must generate enormous data sets.

To begin, we look at at the differential form of the scattering rate. In this case we consider the rate by pieces. The rate from the initial scattering at position (x, y, z) and energy (prior to entering the target), E towards the second scattering position along direction (θ, ϕ) is given by:

$$d\mathcal{R}_1(\vec{v}) = \mathcal{L}_1(x, y, z, E)\sigma_1(z, E, \theta, \phi) \sin\theta d\theta d\phi, \tag{22}$$

d [nm]	$\mathcal{R}_{L_1}$ [Hz/uA]	$\mathcal{R}_{R_1}$ [Hz/uA]	$\mathcal{R}_1^{sim.}$[Hz/uA]
52	5.0±0.1	15.5±0.4	10.3±0.2
100	9.6±0.3	29.8±0.8	19.7±0.4
200	19.3±0.5	59.8±1.7	39.5±0.9
215	20.7±0.6	64.2±1.8	42.5±0.9
300	28.9±0.8	89.7±2.5	59.3±1.3
389	37.5±1.0	116.0±3.2	76.7±1.7
400	38.5±1.1	119.7±3.3	79.1±1.7
487	46.9±1.3	145.5±4.0	96.2±2.1
500	48.2±1.3	149.2±4.2	98.7±2.2
561	54.0±1.5	167.4±4.7	110.7±2.4
600	57.8±1.6	179.2±5.0	118.5±2.6
700	67.4±1.9	209.3±5.8	138.3±3.1
775	74.7±2.1	231.4±6.4	153.0±3.4
800	77.1±2.1	239.2±6.6	158.1±3.5
837	80.6±2.2	249.8±6.9	165.2±3.7
900	86.6±2.4	269.0±7.5	177.8±3.9
944	91.0±2.5	282.2±7.8	186.6±4.1
1000	96.3±2.7	299.5±8.3	197.9±4.4

Table 2: Rates calculated from single scattering simulations of 10^8 thrown events. From left to right: Rate in left detector, rate in right detector, average of the two.

with the luminosity in an infinitesimal volume about the first scattering vertex given by:

$$\mathcal{L}_1(\vec{v}) = \frac{N_A \rho}{A} \frac{N_B}{(2\pi)^{3/2}\sigma_x\sigma_y\sigma_E} \exp\left[-\frac{x^2}{2\sigma_x^2} - \frac{y^2}{2\sigma_y^2} - \frac{E^2}{2\sigma_E^2}\right] dxdydzdE. \tag{23}$$

Similarly the infinitesimal rate our detector sees from the second scattering vertex, a distance, ξ, from the first scattering, towards our detectors at global scattering angle (χ, ψ) is:

$$d\mathcal{R}(\vec{v}) = \mathcal{L}_2(x, y, z, E, \theta, \phi, \xi)\sigma_2(z, E, \xi, \theta, \phi, \chi, \psi)\epsilon(\chi, \psi) \sin\chi d\chi d\psi. \tag{24}$$

The luminosity in this case is

$$\mathcal{L}_2(x, y, z, E, \theta, \phi, \xi) = \frac{N_A \rho}{A} d\mathcal{R}_1(\vec{v}) \exp(-\xi/\lambda) d\xi. \tag{25}$$

where λ is a characterization of to what depth an electron will penetrate in gold. Calculated in the following manner,

$$\frac{1}{\lambda} = 2\pi \frac{N_A \rho}{A} \int_{\pi/2}^{\pi} \sigma(E, \theta) \sin\theta d\theta, \tag{26}$$

we find

$$\lambda = 183\ \mu\text{m}. \tag{27}$$

Since $\lambda \gg d$ we can safely ignore this term in the single scattering case. Additionally, testing has shown that this term has no effect on the resulting rate calculation due to the foil's geometry (only a sliver of events scattered at $\approx \pi/2$ are ever going to have an appreciable amount of foil to travel through) but we include it for completeness' sake. We define

$$f(\vec{v}) = \exp\left[-\frac{x^2}{2\sigma_x^2} - \frac{y^2}{2\sigma_y^2} - \frac{E^2}{2\sigma_E^2}\right] \exp(-\xi/\lambda)\sigma_1(\vec{v})\sigma_2(\vec{v})\epsilon(\chi,\psi)\sin\theta\sin\chi, \tag{28}$$

Which allows us to write our rate integral as:

$$\mathcal{R} = \left(\frac{N_A\rho}{A}\right)^2 \frac{N_B}{(2\pi)^{3/2}\sigma_x\sigma_y\sigma_E} \int_V f(x,y,z,E,\theta,\phi,\xi,\chi,\psi)dv \tag{29}$$

The `GEANT4` simulation samples the double scattering phase space, V, according to the probability density function

$$g(\vec{v}) = C\exp\left[-\frac{x^2}{2\sigma_x^2} - \frac{y^2}{2\sigma_y^2} - \frac{E^2}{2\sigma_E^2}\right]\sin\theta\sin\chi, \tag{30}$$

uniformly sampling all non-explicit variables, with the normalization condition,

$$\frac{1}{C} = \int_V g(x,y,E,\theta,\chi)dv. \tag{31}$$

The integrations over x, y, E, ϕ, ξ, χ, and ψ can be performed trivially, leaving:

$$\frac{1}{C} = (2\pi)^{3/2}\sigma_x\sigma_y\sigma_E\frac{2\pi^2}{9}\left(\cos\frac{\pi}{36} - \cos\frac{\pi}{18}\right)\times I, \tag{32}$$

where we define

$$I = \int_0^d\int_0^\pi \xi_{max}(\theta,z)\sin\theta d\theta dz. \tag{33}$$

In the above equation, $\xi_{max}(\theta,z)$ is the maximum distance between the two scattering vertices can be generated given the initial scattering position and angle. Since the simulation constrains generated electrons to not lose more than 500 keV in the target (these would not be counted in our physical asymmetry in any case), we put a distance limit, $D = 157\,\mu$m, for those particles travelling at $\theta \approx \pi/2$. Thus we define:

$$\xi_{max}(\theta,z) = \begin{cases} \frac{d-z}{\cos\theta}\left[1 - H\left(\frac{d-z}{\cos\theta} - D\right)\right] + DH\left(\frac{d-z}{\cos\theta} - D\right) & \text{if } \theta \leq \pi/2 \\ \frac{-z}{\cos\theta}\left[1 - H\left(\frac{-z}{\cos\theta} - D\right)\right] + DH\left(\frac{-z}{\cos\theta} - D\right) & \text{if } \theta > \pi/2, \end{cases} \tag{34}$$

where $H(x)$ is the Heaviside step function. The integral in Eq. (33) is covered in Appendix A where it is found that $I = d^2$. Thus Eq. 32 becomes

$$\frac{1}{C} = (2\pi)^{3/2}\sigma_x\sigma_y\sigma_E\frac{2\pi^2}{9}\left(\cos\frac{\pi}{36} - \cos\frac{\pi}{18}\right)d^2. \tag{35}$$

Given the definitions above, we can calculate the rate from double scattering

$$\mathcal{R} = \left(\frac{N_A\rho}{A}\right)^2 \frac{N_B}{(2\pi)^{3/2}\sigma_x\sigma_y\sigma_E}\int_V \frac{f(\vec{v})}{g(\vec{v})}g(\vec{v})dv \tag{36}$$

Using the Reimann sum method is not available to us due to the high dimension of the integral and the difficulty of the integration limits We use a Monte Carlo Estimator as described in [1]:

$$\mathcal{R} = \frac{1}{n}\left(\frac{N_A\rho}{A}\right)^2 \frac{N_B}{(2\pi)^{3/2}\sigma_x\sigma_y\sigma_E}\sum_i^n \frac{f(\vec{v}_i)}{g(\vec{v}_i)} \tag{37}$$

$$= \frac{1}{C}\frac{1}{n}\left(\frac{N_A\rho}{A}\right)^2 \frac{N_B}{(2\pi)^{3/2}\sigma_x\sigma_y\sigma_E}\sum_i^n \sigma_1(\vec{v}_i)\sigma_2(\vec{v}_i)\epsilon(\chi_i,\psi_i) \tag{38}$$

$$= \frac{2\pi^2}{9}\left(\cos\frac{\pi}{36} - \cos\frac{\pi}{18}\right) N_B \left(\frac{N_A\rho d}{A}\right)^2 \frac{1}{n}\sum_i^n \sigma_1(\vec{v}_i)\sigma_2(\vec{v}_i)\epsilon(\chi_i,\psi_i) \tag{39}$$

Results of this method are shown in Table 3. We compare the simulated coefficient for quadratic rate scaling:

$$a_2^{sim.} = \left\langle \mathcal{R}_2^{sim.}/d^2 \right\rangle = 62 \pm 15\ \mu\text{Hz}/(\mu\text{A nm}^2), \tag{40}$$

to the result from data in Eq. (14) and find them compatible. However constructing a double scattering asymmetry analagous to Eq. (21) proves problematic. While there is no clear thickness dependence, there is significant variance from point to point which can be seen in Figure 6. We calculate:

$$\varepsilon_2^{rate} = \left\langle \frac{\mathcal{R}_{L_2} - \mathcal{R}_{R_2}}{\mathcal{R}_{L_2} + \mathcal{R}_{R_2}} \right\rangle = 0.28 \pm 0.11. \tag{41}$$

This result is not consistent with the results of the rejection method in 2.2 which is somewhat puzzling and requires further investigation.

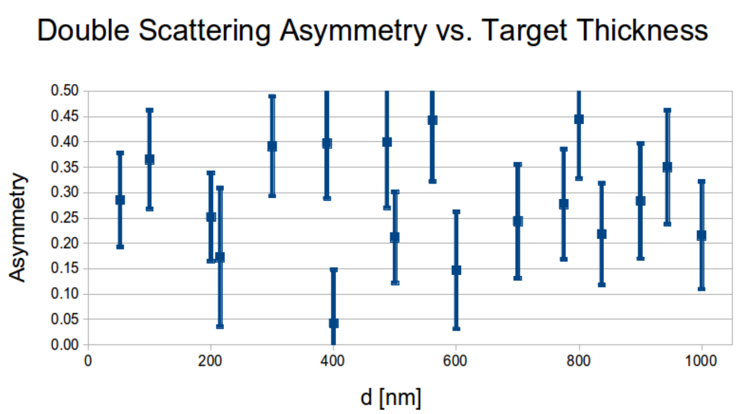

Figure 6: Asymmetry as calculated in Eq. (41) from results of 2.5×10^8 event simulation at each target thickness.

3 Combined Results

With the rates in both left and right detectors for single and double scattering, we can perform comparisons directly to data. The simulation calculates a combined rate of

$$\mathcal{R}_{tot.}^{sim.} = \frac{1}{2}\left[\mathcal{R}_{L_1} + \mathcal{R}_{R_1} + \mathcal{R}_{L_2} + \mathcal{R}_{R_2}\right]. \tag{42}$$

d [nm]	$\mathcal{R}_{L_2}$ [Hz/uA]	$\mathcal{R}_{R_2}$ [Hz/uA]	$\mathcal{R}_2^{sim.}$[Hz/uA]
52	0.22±0.02	0.12±0.02	0.17±0.01
100	0.78±0.09	0.36±0.05	0.57±0.05
200	2.92±0.32	1.74±0.23	2.33±0.20
215	3.79±0.48	2.68±0.73	3.24±0.44
300	8.21±0.97	3.59±0.47	5.90±0.54
389	12.94±1.70	5.58±0.78	9.26±0.93
400	11.25±1.37	10.33±1.83	10.79±1.14
487	20.46±3.09	8.79±1.64	14.63±1.75
500	16.64±1.82	10.82±1.57	13.73±1.20
561	29.69±4.17	11.47±1.83	20.58±2.28
600	28.60±4.33	21.27±3.71	24.94±2.85
700	43.84±4.90	26.69±5.93	35.26±3.85
775	40.56±5.58	22.95±3.63	31.76±3.33
800	67.56±8.87	25.98±4.54	46.77±4.98
837	49.58±6.34	31.81±4.86	40.69±4.00
900	67.97±8.44	37.97±7.92	52.97±5.79
944	77.47±10.19	37.28±6.63	57.37±6.08
1000	76.53±9.86	49.38±8.53	62.95±6.52

Table 3: Rates calculated from double-scattering simulations of 2.5×10^8 thrown events. From left to right: Rate in left detector, rate in right detector, average of the two.

The results of Eq. (42) can be seen compared to data in Table 4.

d[nm]	$\mathcal{R}^{\rm data}$[Hz/μA]	$\mathcal{R}^{\rm sim}_{\rm tot.}$[Hz/$\mu$A]
52	9.93±0.09	10.45±0.23
215	46.50±0.48	45.69±1.03
389	82.58±1.04	85.98±1.94
487	97.74±1.00	110.82±2.75
561	128.66±1.32	131.31±3.34
775	178.30±1.86	184.76±4.75
837	209.30±2.15	205.90±5.41
944	246.00±2.53	243.98±7.34

Table 4: Data rates compared to combined simulation rates.

A combined asymmetry can be constructed in a similar way:

$$A^{sim.} = \frac{[\mathcal{R}_{L_1} - \mathcal{R}_{R_1}] + [\mathcal{R}_{L_2} - \mathcal{R}_{R_2}]}{[\mathcal{R}_{L_1} + \mathcal{R}_{R_1}] + [\mathcal{R}_{L_2} + \mathcal{R}_{R_2}]}, \tag{43}$$

allowing direct comparison with data as in Table 5.

However, the simulation also indicates, without reference to our experimental data, that the single scattering rates scale linearly with thickness and have a thickness-independent asymmetry.

d [nm]	A^{data} [%]	$A^{sim.}$ [%]
52	43.26±0.11	43.0±2.2
215	40.97±0.07	39.9±2.2
389	39.18±0.08	35.6±2.1
487	38.56±0.08	33.8±2.3
561	37.21±0.08	31.2±2.4
775	35.61±0.08	32.4±2.4
837	34.59±0.08	31.6±2.4
944	33.77±0.08	26.6±2.7

Table 5: Asymmetry measured on the target foils compared to combined simulation asymmetry calculated according to Eq. 43.

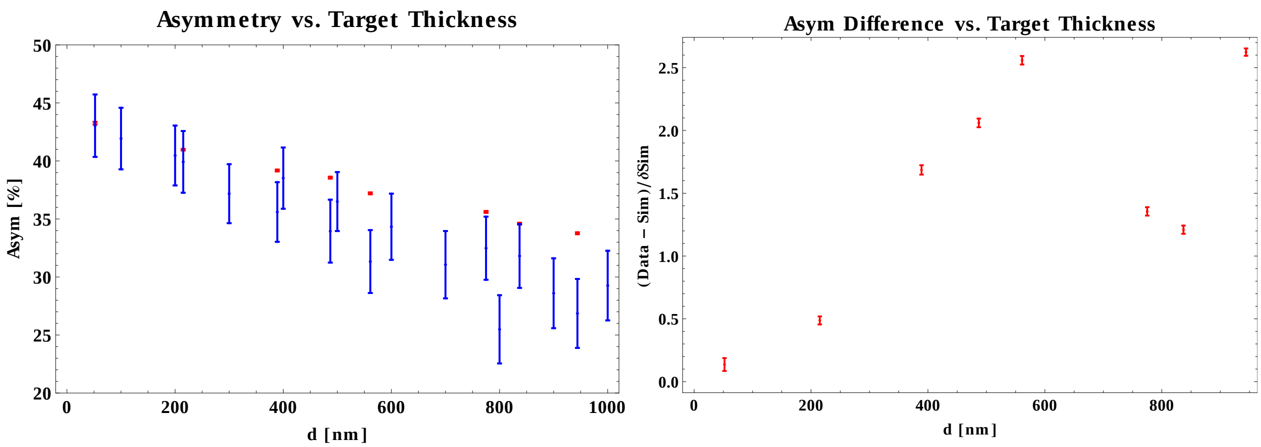

Figure 7: On the left: Combined simulation asymmetries (blue) compared to data (red). On the right, the relative difference between the two given by $(\dashv^{data} - \mathcal{A}^{sim.}(d))/\delta\mathcal{A}^{sim.}(d)$.

Likewise, the double scattering rates scale quadratically while also having a thickness-independent asymmetry. That is to say that we can make the following well founded assumptions:

$$\mathcal{R}_{L_1}(d) = a_1^{sim.} d(1 + P\varepsilon_1) \qquad \mathcal{R}_{R_1}(d) = a_1^{sim.} d(1 - P\varepsilon_1)$$
$$\mathcal{R}_{L_2}(d) = a_2^{sim.} d^2(1 + P\varepsilon_2) \qquad \mathcal{R}_{R_2}(d) = a_2^{sim.} d^2(1 - P\varepsilon_2)$$

Which, when inserted into Eqs. (42 - 43), lead to analytic predictions (based solely on simulation outputs) for the rate

$$\mathcal{R}^{pred.}(d) = a_1 d + a_2 d^2 \tag{44}$$

and the asymmetry (which does rely on knowledge of P)

$$A^{pred.}(d) = P\frac{a_1\varepsilon_1 + a_2\varepsilon_2 d}{a_1 + a_2 d} \tag{45}$$

respectively. Thus we have a prediction for the effective Sherman function using only simulation derived values:

$$\boxed{S_{eff}^{pred.}(d) = \frac{a_1\varepsilon_1 + a_2\varepsilon_2 d}{a_1 + a_2 d}}. \tag{46}$$

Additional details can be seen in Figure 8.

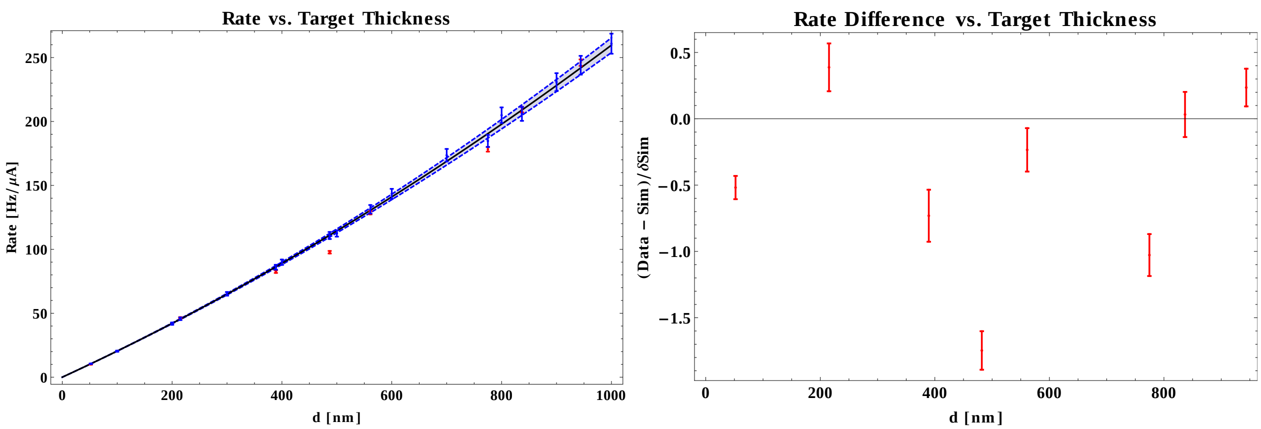

Figure 8: On the left: Combined simulation rates (blue) compared to data rates (red). The black curve is the analytic simulation prediction from Eq. 44. On the right, the relative difference between the two given by $(\mathcal{R}^{data} - \mathcal{R}^{pred.}(d))/\delta\mathcal{R}^{pred.}(d)$ incorporating the uncertainty of the measured target thickness.

4 Conclusions

The Mott GEANT4 simulation has lead to a theory driven prediction for the form of the effective Sherman function. However, some investigation is required in order to resolve the apparent discrepancy between $\varepsilon_2^{rej.}$ and ε_2^{rate}. This form of the effective Sherman function also indicates a new, theory based, fitting formula for extrapolation from finite target thickness to zero:

$$A^{fit}(d) = \frac{A_0 + \alpha d}{1 + \beta d}. \tag{47}$$

We can compare this fit to the simulation predictions using:

$$A_0 = P\varepsilon_1 \tag{48}$$
$$\alpha = Pa_2\varepsilon_2/a_1 \tag{49}$$
$$\beta = a_2/a_1 \tag{50}$$
$$\tag{51}$$

The results of this fit can be seen next compared to the simulation based prediction in Figure 9.

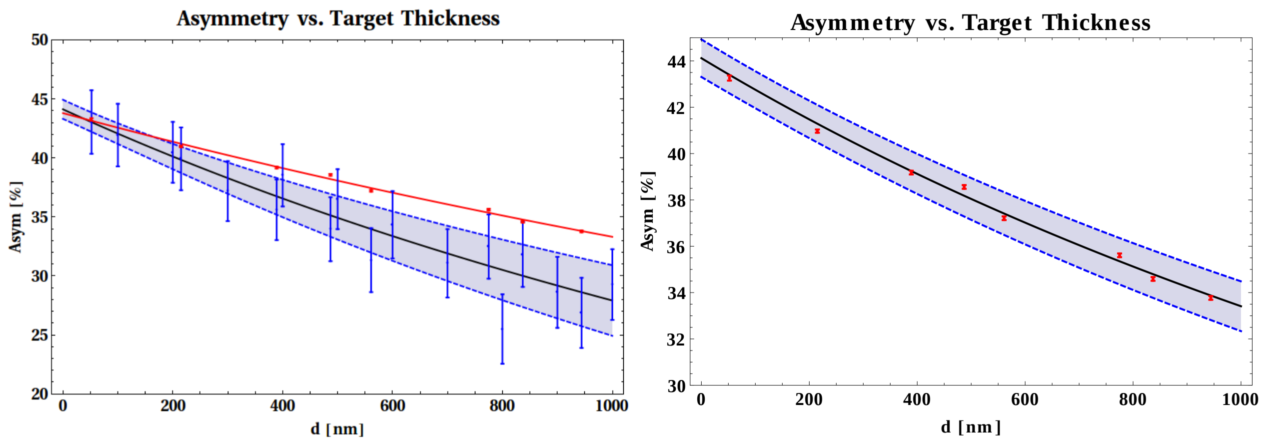

Figure 9: Left: Combined simulation asymmetries (blue) compared to data rates (red). The black curve is the analytic simulation prediction from Eq. 44 using $\varepsilon_2^{rate} = 0.28 \pm 0.11$. The red curve is a fit using Eq. 47. Right: Data (red) is matched to the prediction from Eq. 44 using $\varepsilon_2^{rej} = 0.011 \pm 0.003$.

References

[1] Malvin H. Kalos and Paula A. Whitlock. *Monte Carlo Methods*. WILEY-VCH Verlag GmbH & Co. HGaA, Weinheim, Germany, 2004.

[2] Daniel Moser. Calculating rates. `https://wiki.jlab.org/ciswiki/images/e/ef/Rates.pdf`, 2015.

[3] Xavier Roca-Maza. Mott polarimetry at jlab: Working notes on theory. `https://www.dropbox.com/home/Mott%20Team%20Team%20Folder/Theory?preview=mott-theory.pdf`, 2015.

Appendix A: Normalization Integral

Herein we perform the explicit integration of Eq. (33):

$$I = \int_0^d \int_0^\pi \xi_{max}(\theta, z) \sin\theta d\theta dz. \tag{52}$$

Examining the integral over θ we see

$$\int_0^\pi \xi_{max}(\theta, z) \sin\theta d\theta = (d-z) \int_0^{\alpha_1} \tan\theta d\theta + D \int_{\alpha_1}^{\alpha_2} \sin\theta d\theta + (-z) \int_{\alpha_2}^{\pi} \tan\theta d\theta, \tag{53}$$

where $\cos\alpha_1 = (d-z)/D$ with $0 \leq \alpha_1 < \pi/2$ and $\cos\alpha_2 = -z/D$ with $\pi/2 \leq \alpha_2 < \pi$. We then see:

$$(d-z) \int_0^{\alpha_1} \tan\theta d\theta = -(d-z)\log(\frac{d-z}{D}), \tag{54}$$

$$D \int_{\alpha_1}^{\alpha_2} \sin\theta d\theta = d, \tag{55}$$

$$-z \int_{\alpha_2}^{\pi} \tan\theta d\theta = z\log(\frac{z}{D}), \tag{56}$$

$$\therefore \int_0^\pi \xi_{max}(\theta, z) \sin\theta d\theta = d\left[1 - \log(\frac{d-z}{D})\right] + z\left[\log(\frac{d-z}{D}) + \log(\frac{z}{D})\right]. \tag{57}$$

Therefore we see

$$I = \int_0^d \left(d\left[1 - \log(\frac{d-z}{D})\right] + z\left[\log(\frac{d-z}{D}) + \log(\frac{z}{D})\right]\right) dz \tag{58}$$

$$= d^2 \tag{59}$$

regardless of our initial choice of D (so long as it is a physically possible value).

Appendix B: Error Propagation

From Eq. (44) we obtain an uncertainty:

$$(\delta \mathcal{R}^{pred.})^2 = d^2 \delta {a_1}^2 + d^4 \delta {a_2}^2 + (a_1 + a_2 d)^2 \delta d^2. \tag{60}$$

From Eq. (45) we obtain an uncertainty:

$$(\delta A^{pred.})^2 = (\delta A^{pred.})^2 \delta P^2 + \tag{61}$$